Main Manuscript for

Structural insights into peptidoglycan hydrolysis by the FtsEX system in *Escherichia coli* during cell division

Jianwei Li[1, #], Yutong He[1, #], Xin Xu[1, #], Martin Alcorlo[2], Jian Shi[3], David I. Roper[4], Juan A. Hermoso[2], Lok-To Sham[5], and Min Luo[1, 3, *]

[1] Department of Biological Sciences, Faculty of Science, National University of Singapore

[2] Department of Crystallography and Structural Biology, Instituto de Química-Física "Blas Cabrera", CSIC, Madrid, Spain

[3] Center for Bioimaging Sciences, Department of Biological Sciences, National University of Singapore

[4] School of Life Sciences, University of Warwick, Coventry, CV4 7AL, UK

[5] Infectious Diseases Translational Research Programme and Department of Microbiology and Immunology, Yong Loo Lin School of Medicine, National University of Singapore

[#] These authors contributed equally.

* Corresponding author. Email : dbslmin@nus.edu.sg

Author Contributions: Jianwei Li and Yutong He performed biochemical reconstitution, functional characterization, and cryo-EM studies; Xin Xu performed kinetics assays; Martin Alcorlo, David Roper, Juan A. Hermoso and Lok-To Sham helped with data analysis; Jian Shi helped with EM data collection; Min Luo designed and supervised research, analyzed data, and wrote the paper with help from all authors.

Competing Interest Statement: Authors declare no competing interests.

Classification: Biological Sciences; Microbiology

Keywords: cell division, peptidoglycan, antimicrobial, cryo-EM

This PDF file includes:

Main Text

Figures 1 to 6

Abstract

Bacterial cell division relies on precise peptidoglycan (PG) remodelling, a process orchestrated by the FtsEX complex. Comprised of FtsE and FtsX, this complex collaborates with EnvC, a periplasmic lytic enzyme activator, to regulate septal PG hydrolysis by amidases like AmiB. While recent structural investigations, particularly of *Pseudomonas aeruginosa* FtsEX (*Pae*FtsEX), have shed light on complex interactions and proposed activation mechanisms, the structural intricacies governing PG degradation by the FtsEX complex and EnvC in *Escherichia coli* cytokinesis remain unexplored. In this study, we present a comprehensive biochemical and structural analysis of *E. coli* FtsEX complexes, unveiling a key role for ATP in complex stabilization that extends across bacterial species. Upon EnvC binding, ATPase activity markedly increases. High-resolution structures of *Eco*FtsEX, both in the presence and absence of EnvC, reveal a symmetrical conformation of *Eco*FtsEX capable of accommodating the inherent asymmetry of EnvC, mediated by flexible loops within the periplasmic domain. Our negative-staining imaging showcases an elongated *Eco*FtsEX/EnvC/AmiB complex reminiscent of the *Pae*FtsEX system. These findings collectively provide intricate insights into the regulation of PG cleavage by FtsEX in *E. coli* - a pivotal model system used in pilot genetic studies, suggesting a conserved mechanism for precise hydrolase activation in bacteria.

Introduction

In most bacteria, peptidoglycan (PG) is remodelled during cytokinesis in a highly coordinated fashion. This coordination ensures the daughter cells are separated without causing lethal lesions of PG (1-3). At least 10 essential proteins are involved in cell division in the model organism *Escherichia coli*, many of which are organized by the cytoskeletal protein FtsZ (4, 5). FtsZ recruits FtsA and FtsEX to form the early divisome. After a short pause, the early divisome recruits other division proteins such as FtsK, FtsQLB, FtsWI, and FtsN to the septum (4, 6). The arrival of FtsN somehow triggers cell constriction, likely through activating the FtsQLB complex and FtsA (4, 7-9). Cell separation is then achieved through the amidases AmiA, AmiB, and AmiC. To control their PG hydrolytic activity, these amidases are activated by coiled-coil domain proteins EnvC (for AmiA and AmiB) and NlpD (for AmiC) (1, 3, 10, 11). If these systems are simultaneously inactivated, the daughter cells will be unable to separate and form long chains (12).

PG remodelling is linked to cytokinesis by an ATP-binding cassette (ABC) transporter-like protein complex FtsEX. Rather than transporting a substrate, the FtsEX complex transduces conformational changes that span the cytoplasmic membrane (13, 14). Driven by ATP hydrolysis of FtsE, these changes are required for stimulating EnvC/AmiA/AmiB activities (15, 16) and initiating cell constriction via FtsA (15, 17-19). The FtsEX complex also recruits other cell division

68 proteins to the divisome (17, 19). Thus, deletions of *ftsEX* result in non-viable cells unless they are
69 grown in permissive conditions, such as at a low temperature or in media with high osmolarity (20,
70 21). Alternatively, the essentiality of *ftsEX* can be bypassed by gain-of-function mutations that
71 strengthen the interaction between FtsN and FtsA (17, 20).
72
73 Several partial structures of the FtsEX complex have been reported, some are with their interacting
74 partners (22-25). Very recently, progress has been made in elucidating the full-length structure of
75 the FtsEX complex from *Pseudomonas aeruginosa* (*Pae*FtsEX), both in the presence and absence
76 of critical regulators like ATP, EnvC, and AmiB (26). These structures offer insight into the interfaces
77 between FtsE, FtsX, and their binding partners. In addition, they suggest a mechanism in which
78 the rearrangement of regulatory helices of EnvC and AmiB activates peptidoglycan hydrolysis at
79 the septum (26). Yet, the majority of work regarding FtsEX was done in *Escherichia coli* (15-21),
80 where an abundance of genetic studies has laid a significant foundation for our understanding of
81 PG degradation activation in bacterial cell division. However, the intricate molecular basis
82 orchestrating this process remains elusive, underscoring the need for a direct structural and
83 biochemical investigation within this extensively studied model system. Specifically, given the
84 relatively low sequence similarity between the FtsEX complexes from these two species, it is
85 unclear whether the structural information of *Pae*FtsEX can reconcile the findings from genetic
86 studies. Furthermore, previous genetic studies have proposed a direct interaction between FtsEX
87 and components of the constriction ring, such as FtsA and FtsZ (18, 27), to ensure the accurate
88 localization of FtsEX at the division site. However, there is currently a lack of supporting
89 biochemical and structural evidence in this regard.
90
91 In this study, we present a comprehensive analysis of the structure and function of the *Escherichia*
92 *coli* FtsEX complex (*Eco*FtsEX) in conjunction with EnvC, focusing on its regulation of AmiB
93 activation for PG cleavage. Our investigation uncovers a previously unrecognized function of ATP
94 in stabilizing the FtsEX complex, a role that appears to be conserved across different bacterial
95 species. Notably, we observe a substantial increase in the ATPase activity of *Eco*FtsEX upon
96 binding with EnvC. High-resolution structures of *Eco*FtsEX alone and with EnvC were obtained at
97 3.9 and 3.4 Å, respectively, offering insights into the EnvC recognition mechanism. Interestingly,
98 *Eco*FtsEX maintains a symmetrical conformation even when complexed with the asymmetrical
99 EnvC. Comparative analyses identify the periplasmic domain's flexible loops as key to EnvC
100 interaction, revealing structural adaptability. Furthermore, our negative-staining imaging
101 experiments unveil an elongated conformation of the *Eco*FtsEX/EnvC/AmiB complex for PG
102 cleavage, reminiscent of the FtsEX system from *Pseudomonas aeruginosa*. Together, our results
103 revealed a detailed regulation of PG cleavage by FtsEX in the key model system of *E. coli*,
104 suggesting a conserved mechanism for hydrolase activation in bacteria.

Results

ATP Binding as a Universal Stabilizing Factor for the FtsEX Complex

In our efforts to reconstitute the full-length *Eco*FtsEX complex in vitro, we explored various strategies involving changing the expression constructs and extraction conditions. During the purification process, we observed that the protein remained stable in the presence of 10% glycerol. However, almost all protein precipitated out after the removal of glycerol either through size-exclusion chromatography (SEC) or during the peptidisc reconstitution (**Figure 1A**). This indicated a low level of stability for the complex. To investigate whether the stability of the FtsEX complex might be dependent on its cognate partner, EnvC, we conducted co-expression experiments by introducing EnvC along with FtsE and FtsX (**Figure 1A**). Despite the presence of EnvC, FtsEX still exhibited a tendency to precipitate.

Given the persistent challenges in achieving a stable FtsEX complex, we redirected our focus towards exploring the potential role of the substrate ligand, ATP, in complex stabilization. ATP, well-known for its role as a biological energy source, has also been associated with the stabilization of proteins, as reported in recent studies (28, 29). To investigate this hypothesis, we conducted a series of experiments to assess the impact of ATP on the FtsEX or the FtsEX/EnvC complex (**Figure 1A**). Remarkably, the introduction of ATP resulted in the formation of a robust *Eco*FtsEX complex, both in its standalone form and in the presence of EnvC. This complex remained tightly associated throughout the SEC process (**Figure supplement 1A**). Further validation through negative-staining electron microscopy confirmed that the purified *Eco*FtsEX complex maintained stability, with clearly discernible features corresponding to an intact ABC transporter containing two FtsE and two FtsX subunits (**Figure 1B**). This compelling evidence suggests that ATP, acting as the substrate of FtsEX, also plays a pivotal role in stabilizing this crucial complex formation.

Interestingly, ATP analogues, including ATPγS, AMP-PNP, and ADP, also exhibited similar stabilizing effects (**Figure 1C**). As they are not hydrolysable for FtsEX, it indicates that ATP binding, rather than hydrolysis, is sufficient for complex stabilization. This was corroborated by the introduction of a FtsE mutant (E163Q), inspired by related ABC transporters (26), which is incapable of ATP hydrolysis. When this mutant was assessed for complex formation with FtsX in the presence of ATP, it indeed formed a stable complex (**Figure 1C**). These findings suggest ATP binding alone is responsible for stabilizing the complex formation.

To expand the scope of our investigation, we explored whether ATP could similarly stabilize FtsEX complexes from other bacterial species, which had also presented challenges in in-vitro reconstitution. We expressed and purified FtsEX from various species, including *Streptococcus*

142 *pneumoniae, Pseudomonas aeruginosa*, and *Bacillus subtilis,* in the presence and absence of ATP.
143 Remarkably, regardless of the bacterial species, ATP consistently enhanced the stability of the
144 complexes, as demonstrated by either increased complex yield in SEC elution profiles or with a
145 more accurate stoichiometry between FtsE and FtsX as shown from the SDS-page gel (**Figure**
146 **supplement 1B**). Collectively, our findings underscore the pivotal role of ATP in stabilizing FtsEX
147 complexes. Notably, the ability of other nonhydrolizable ATP analogues to replicate this effect
148 suggests that ATP binding is a crucial step required to facilitate the coupling of FtsX and FtsE for
149 the formation of a functionally stable complex.
150
151 **Biochemical Characterization of FtsEX and Its Complexes with EnvC in *E. coli***
152 The His-tagged full-length FtsE and FtsX proteins from *E. coli* (str. K-12, MG1655) were
153 overexpressed in *E. coli* BL21(DE3) and subsequently purified using a combination of affinity and
154 size-exclusion chromatography (SEC) (**Figure supplement 1A**). For subsequent functional and
155 structural investigations, FtsEX was solubilized in DDM and reconstituted into peptidiscs (see
156 Methods). Given the proven stabilization role, 0.5 mM ATP was maintained throughout the entire
157 purification process of *Eco*FtsEX.
158
159 Assays assessing ATPase activity demonstrated that, in contrast to previously reported FtsEX
160 complexes from *Pseudomonas aeruginosa*, the *Eco*FtsEX complex exhibited obvious basal
161 ATPase activity (**Figure 1D**). To confirm this, we introduced the FtsE mutant (E163Q) as a control,
162 which was not able to hydrolyse ATP. As anticipated, ATPase activity in the mutant was markedly
163 diminished (**Figure 1D**), while low ATPase activity was still detected, potentially attributable to co-
164 purified proteins.
165
166 To understand the role of ATP binding/hydrolysis on EnvC recruitment, a protein pull-down assay
167 was conducted. As ATP was present in the purified protein, a wash step with buffer in the presence
168 of Mg^{2+} and 10% glycerol was performed to remove the extra ATP for the FtsEX complex that bind
169 to the resin. Next, bound FtsEX and EnvC were mixed in the presence of ATP or its non-
170 hydrolysable analogue, ATPγS (**Figure 1E**). The results revealed that EnvC stably associated with
171 FtsEX, with its binding seemingly unaffected by ATP hydrolysis. This was evidenced by the
172 comparable amounts of EnvC bound in the presence of 3 mM ATPγS and 3 mM ATP. To confirm
173 this, $FtsEX^{E163Q}$ mutant was introduced. Results, similar to those from the wild type, showed that
174 the mutant still demonstrated similar EnvC binding levels. This confirms that ATP binding is
175 sufficient to initiate EnvC recruitment.
176
177 Additionally, the effects of EnvC binding on the ATPase activity of *Eco*FtsEX were probed (**Figure**
178 **1D**). An enhanced activity was observed upon the addition of EnvC. This EnvC-mediated increase

179 in ATPase activity was further validated through ATPase assays involving varying ATP
180 concentrations for both FtsEX and the FtsEX/EnvC complex. Both sets of data fit well with the
181 Michaelis-Menten equation (**Figure 1F**). Notably, in the presence of EnvC, the V_{max} (92.7±5.1
182 nmol/mg/min) was approximately 2.2-fold higher than that observed for FtsEX (42.7±2.1
183 nmol/mg/min) alone. However, no large differences were observed regarding the K_m (0.11±0.02
184 mM for FtsEX/EnvC; 0.13±0.02 mM for FtsEX). Together, these findings underscore that in the
185 presence of ATP, FtsEX and EnvC form a robust complex; while *Eco*FtsEX inherently exhibits
186 ATPase activity, the presence of EnvC stimulates this activity.
187
188 **CryoEM structure of *Eco*FtsEX reveals a symmetrical PLD arrangement**
189 To elucidate the full-length structure of *Eco*FtsEX, we subjected the WT *Eco*FtsEX sample,
190 incubated with 3 mM ATPγS, to single-particle CryoEM analysis and achieved a resolution of 3.7 Å
191 (**Figure supplement 2**). This map was of sufficient resolution for detailed model-building for the
192 Transmembrane domains (TMD), the nucleotide-binding domains (NBD), and a large portion of the
193 Periplasmic domain (PLD); in addition, density for two bound nucleotides was clearly captured as
194 well (**Figure supplement 3A**).
195
196 *Eco*FtsEX, akin to most Type VII ABC transporters, possesses one coupling helice (CH) and a C
197 terminal tail (C-tail) (**Figure 2A**). Cryo-EM structure reveals the assembly of the full *Eco*FtsEX
198 system (**Figure 2B**). This comprises two cytosolic FtsE NBD domains and two FtsX, with TMD
199 domains embedded in the membrane and PLD extending into the periplasmic space. Both TMD
200 and NBD regions in the *Eco*FtsEX structure exhibit canonical folds, similar to other characterized
201 Type VII ABC transporters such as MacB, LolCDE, and *Pae*FtsEX. The overall conformation of
202 *Eco*FtsEX is quite similar to that of *Pae*FtsEX (**Figure supplement 3B**). Notably, the N-terminal
203 region of FtsX (Residues 53-70) forms an elbow helix (EH) oriented parallel to the membrane
204 (**Figure 2B**). Like its counterpart in *Pae*FtsEX, the extreme N-terminal region of FtsX (Residues 1-
205 52) was not resolved, suggesting its highly disordered nature.
206
207 The entire PLD domain comprises a smaller loop and a larger domain. For ease of reference, only
208 the larger domain is termed the PLD (**Figure 2A**). The smaller loop encompasses 14 residues
209 between TM3 and TM4. The principal PLD domain, spanning residues between TM1 and TM2
210 (106-208), displays a canonical topology, with a Porter domain and an X-lobe (14, 22). Compared
211 to the TMD and NBD regions, PLD domains exhibit higher flexibility, evident from their diminished
212 EM density at a contour level of 0.22 in Chimera. Lowering the contour to 0.1 in Chimera reveals
213 clear density, enabling the visualization of PLD's secondary structures (**Figure supplement 2F**),
214 with an exception for the X-lobe segment with residues 161-168 (**Figure 2C**). Structurally, the
215 individual PLD domains are superimposable (**Figure 2C)**, and also align closely with those in

216 *Pae*FtsEX (**Figure supplement 4**), despite their amino acid sequence identities with *E. coli* being
217 only 29%.
218
219 The PLD domain of *Eco*FtsEX structure offers a snapshot with well-defined secondary structures,
220 highlighting a 2-fold symmetrical conformation (**Figure 2D)**. The X-lobes of both PLDs are oriented
221 mutually inwards with sideways blocked and appear to facilitate EnvC binding strictly from the top
222 of the FtsEX complex, mirroring findings in the *Pae*FtsEX system.
223
224 **CryoEM structure of *Eco*FtsEX/EnvC Complex elucidates EnvC binding and ATP-Dependent**
225 **LytM Release**
226 To elucidate the EnvC recruitment by FtsEX in *E. coli*, purified FtsEX^{E163Q} mutant was reconstituted
227 in peptidiscs and incubated with EnvC in the presence of 2 mM ATP for cryo-EM analysis (**Figure**
228 **supplement 5**). After 3D reconstruction, a major conformation stands out with resolution
229 determined at 3.4 Å (**Figure supplement 5F**). The quality of the EM density allowed modelling of
230 nearly all sidechains of FtsEX, the two bound nucleotides, and a portion of EnvC's coiled-coil
231 domain (CCD) (**Figure 3A & Figure supplement 6**). The density of EnvC's remaining regions,
232 including part of the CCD domain, the LytM domain and the regulatory helix, was absent,
233 suggesting significant flexibility. The global configuration of the FtsEX/EnvC complex is similar to
234 the previously described *Pae*FtsEX system (**Figure supplement 7**), where EnvC inserts from
235 above between the two PLD domains along the FtsEX central axis.
236
237 To dissect the state of the bound EnvC, we compared our cryoEM FtsEX/EnvC complex with the
238 crystal structure of the PLD domain in complex with EnvC (PLD/EnvC) from *E. coli* (PDB code:
239 6TPI) *(22)*, where EnvC was in an inactivated state. In the PLD/EnvC structure, a distinct
240 asymmetrical conformation is evident: one PLD is positioned about 5 Å higher than the other one,
241 accommodating the bound asymmetric EnvC with its LytM domain locked (**Figure supplement 8A,**
242 **left**). However, in our full-length ATP-bound FtsEX/EnvC structure, the two PLDs are highly
243 symmetrical (**Figure supplement 8A, right**). Besides this, the bound EnvC has also undergone
244 conformational shifts (**Figure supplement 8B**). In contrast to the PLD/EnvC crystal structure,
245 where the two CCD helices exhibit huge asymmetry (**Figure supplement 8B, left**), our structure
246 reveals a more symmetrical arrangement induced by simultaneous compression from both PLD
247 domains (**Figure supplement 8B, right**). Consequently, the distance between the terminal residue
248 of the α1 helix (Q127) and the initial residue of the α2 helix (Q143) within the CCD domain is
249 reduced from 24 Å to a mere 10 Å, while residing at a relatively similar height from the PLD domain.
250 This compression of the CCD helices may drive the release of the LytM domain, supported by the
251 lack of LytM density in our EM map. Together, we hypothesize that in the presence of ATP, the
252 LytM domain is released, facilitating AmiB recruitment.

253

254 **Detailed EnvC interactions with FtsEX**

255 The ATP-bound *Eco*FtsEX/EnvC structure also revealed detailed interactions with EnvC. This
256 interaction mainly involves two interfaces and covers an approximate surface area of 2290 $Å^2$,
257 predominantly consisting of hydrophobic contacts (**Figure 3B**).

258

259 The primary interface, also resolved in the PLD/EnvC crystal structure (22), features residues Y114,
260 F152, W155, F158, L162, L165, and L170 of FtsX associating with residues L117, L121, L148,
261 Y151, F152, Y154, L155, and I163 of EnvC (**Figure 3C**). Conversely, the secondary interface
262 encompasses the Lip of CCD from EnvC, and the small loop of FtsX. Interacting residues at this
263 interface comprise I133, L135, I136, L137, E141 from EnvC and W210, L214, F309 from FtsX.
264 Although hydrophobic interactions dominate, several electrostatic interactions exist, notably the
265 salt bridges ($R126_{EnvC}$-$D207_{FtsX}$, $E141_{EnvC}$-$R213_{FtsX}$) (**Figure 3D**). These interactions have largely
266 been validated by previous studies (22), mutations like Y114E, F152E, and L165A in FtsX's
267 periplasmic domain notably affected EnvC's binding efficacy, affirming their role in recruiting EnvC.

268

269 **Recognition of Asymmetrical EnvC by Symmetrical FtsEX: Unveiling Key Loops for**
270 **Conformational Adaptivity**

271 Intriguingly, our analysis of the FtsEX/EnvC structure showed that even when bound to the
272 asymmetrical EnvC, FtsEX—including its two PLD domains interacting directly with EnvC—
273 maintains a symmetrical conformation (**Figure 4A**). Compared to the *Eco*FtsEX structure without
274 EnvC, which is also symmetrical, the only noticeable change is the outward shift of the two PLD
275 hooks by about 12 Å (**Figure 4A**), a result of their interaction with the CCD domain of EnvC (**Figure**
276 **4B**). This observation poses an interesting question: How does the inherently symmetrical FtsEX
277 cater to an asymmetrical binding partner? To explore this, we closely analysed the FtsX-EnvC
278 binding interface.

279

280 Upon detailed examination, we noticed that the motifs in FtsEX directly interacting with EnvC are
281 primarily loops (**Figure 4C**). The main loop engaging with EnvC is X-lobe (**Figure 4D**), covering
282 residues G157-L171. This segment, originally disordered in the FtsEX alone structure, becomes
283 crucial for engaging with EnvC, involving a binding interface of about 1204 $Å^2$. The other interacting
284 regions are loops spanning residues Y104-Q109 (**Figure 4E**) and D208-L214 (**Figure 4F**), and a
285 segment of the small loop in the PLD domain (Q307-T311) (**Figure 4G**). Combined, these loops
286 (eight in total from the two PLD domains) are responsible for the majority of the interactions with
287 EnvC. This inherent adaptability in the loops provides FtsEX the versatility needed for binding the
288 asymmetrical EnvC. Notably, the interactions contributed by these loops are largely hydrophobic
289 (**Figure 4D-G)**. Thus, our data suggest that the flexible loops, along with the hydrophobic

interactions they facilitate, equip the symmetrical FtsEX to effectively engage with asymmetrical partners.

Reconstitution and Elucidating the Elongated Conformation of *E. coli* FtsEX/EnvC/AmiB Complex for PG cleavage

The absence of the LytM density, in comparison to the crystal structure of PLD/EnvC (22), indicates that our ATP-bound FtsEX/EnvC sample likely has the LytM domain released, primed for hydrolase interaction. To further validate this, we conducted pull-down assays (**Figure 5A**). When we incubated AmiB with either the FtsEX/EnvC complex or the mutant FtsEX^{E163Q}/EnvC in the presence of ATP or its nonhydrolyzable analogue, ATPγS, both the wild type and mutant FtsEX/EnvC complexes effectively pulled down AmiB. Notably, ATP and ATPγS showed similar levels of AmiB binding, confirming that ATP-bound FtsEX/EnvC is prepped for AmiB recruitment. Additionally, we investigated the influence of AmiB binding on FtsEX's ATPase activity (**Figure 5B**). There was no obvious effect upon the addition of AmiB to the FtsEX/EnvC complex, suggesting that AmiB does not regulate FtsEX function.

Next, we sought to check if the bound AmiB is activated for PG cleavage. FtsEX/EnvC complex was first mixed with a threefold molar excess of AmiB in the presence of 2 mM ATP, and the mixture was applied to size-exclusion chromatography (SEC) (**Figure 5C**). An early eluting fraction was observed, and subsequent SDS-PAGE confirmed the co-existence of FtsE, FtsX, EnvC, and AmiB in this fraction. The reconstituted PG-cleaving complex of *Eco*FtsEX/EnvC/AmiB, was further analysed using negative staining (NS) electron microscopy (**Figure 5D**). Many of the observed particles exhibited long tails in the image, a feature suggestive of AmiB binding. A 2D classification analysis presented an elongated structure, mirroring previous observations in *P. aeruginosa* (26). The electron densities on the periplasmic side displayed a distinct rod-like form in alignment with the FtsEX complex's central axis, extending about 290 Å into the periplasm, which we attribute to the bound EnvC and AmiB. This conformation likely represents an activated state prepared for PG cleavage. However, due to the *Eco*FtsEX complex's instability during the PG hydrolysis assay, we couldn't directly check PG cleavage activity. The attempt to obtain a CryoEM structure of the complex was also unsuccessful, possibly because of its inherent flexibility, preventing the reconstruction of a clear EM map. Nonetheless, it has been well established in *P. aeruginosa*, where the active FtsEX/EnvC/AmiB complex also assumes an extended form (**Figure 5E**), we propose that our observed complex with a similar conformation is also in an activated state, primed for PG degradation.

Discussion

326 A structural and functional description is here provided for the complete *E. coli* lytic machinery
327 regulated by the FtsEX system. We observed an antiparallel arrangement of PLDs in the
328 periplasmic space in the *Eco*FtsEX complex. Incorporation of ATP, but not hydrolysis, is capable
329 of facilitating EnvC binding. The ternary complex increases its ATPase activity, compared with that
330 of the binary complex. Interestingly, upon ATP binding, the flexibility of loops in the PLD domain
331 allows a symmetric interaction with the EnvC coiled-coil domain that is compressed to allow the
332 release of its LytM domain. While resolution for the complete FtsEX/EnvC/AmiB complex limited
333 detailed descriptions, our cryo-EM data points to a very similar disposition of the lytic complex to
334 that reported for *P. aeruginosa* (26) with a fully expanded EnvC coiled-coil that would place the
335 amidase at ~300 Å over the inner membrane.
336
337 In the context of recruiting an asymmetric partner by the inherently symmetrical FtsEX complex,
338 our study has unveiled a dynamic and intriguing mechanism. At the centre of this mechanism lies
339 the highly flexible PLD domain (composed of the porter domain and the loops connecting the
340 different TM of FtsX), which demonstrates exceptional adaptability due to the presence of multiple
341 flexible loops, including the x-lobe. These flexible loops within the PLD domain function as dynamic
342 connectors, enabling the FtsEX complex to finely tune its conformation and engage with
343 asymmetric partners in an exceptionally adaptable manner. This inherent plasticity empowers the
344 FtsEX complex to align itself with the specific structural requirements of its binding partners, thereby
345 facilitating their effective interaction and subsequent regulatory processes.
346
347 Moreover, these flexible elements serve a dual role by providing the necessary adaptability to
348 bridge the gap between the inherent symmetry of the FtsEX complex and the asymmetry present
349 in its interacting partners. This becomes particularly intriguing in the context of bacterial cell
350 division, where the same FtsEX complex must interact with a variety of asymmetric binding
351 partners. These binding partners exhibit diverse structural features and distinct binding interfaces,
352 necessitating a mechanism that allows the inherently symmetrical FtsEX complex to engage with
353 them with precision and effectiveness.
354
355 Our study has uncovered a previously unrecognized role of ATP in the stabilization of the FtsEX
356 complex, a role that extends beyond its established function as a substrate. This discovery not only
357 expands our understanding of the functional versatility of ATP but also unravels a crucial aspect of
358 how FtsEX complexes are regulated. The stabilizing influence of ATP is particularly intriguing, as
359 evidenced by our experiments across diverse bacterial species, suggesting that ATP-driven
360 stabilization might represent a shared feature among FtsEX complexes in various bacteria.
361 Furthermore, it is noteworthy that both the FtsEX systems from *E. coli* and the recently
362 characterized system from *P. aeruginosa* exhibit a relatively low basal ATPase activity. However,

363 this activity is significantly enhanced in the presence of their respective cognate binding partner,
364 EnvC. Specifically, for *E. coli*, the ATPase activity increases by a factor of 2.2, whereas for *P.*
365 *aeruginosa*, the increase is even more pronounced, with a greater than 20-fold enhancement
366 observed. This additional regulatory mechanism ensures that, under normal physiological
367 conditions, minimal energy is expended. It is only during the cell division process, when
368 components like EnvC are involved, that the ATPase activity of FtsEX becomes fully activated.
369
370 Interestingly, our cryoEM map of EcoFtsEX, expressed from its native host bacteria *E. coli*,
371 revealed an additional density located on the bottom side of the complex adjacent to FtsE (**Figure**
372 **supplement 2**, and **Figure supplement 9A**). This suggests the co-purification of endogenously
373 binding proteins with the complex. To identify the proteins, we conducted mass spectrometry on
374 the purified FtsEX sample. Our results showed that in addition to FtsE and FtsX, FtsA was present
375 in significant abundance, followed by FtsZ (**Figure supplement 9B**). This observation is consistent
376 with previous genetic and phenotypic observations on the *E. coli* divisome activation (17, 27). We
377 also noted during the course of these studies that the interaction of *E.coli* FtsA with FtsEX protein
378 complexes from other species is indicative of the conserved and fundamental nature of divisome
379 protein interactions. For example, the overexpression of *S. pneumoniae* FtsEX in *E. coli* also
380 indicated an association with *E.coli* FtsA and could be isolated using styrene-maleic acid isolation
381 and affinity purification as shown in **Figure supplement 9C** (30, 31). If this holds true, it would
382 provide a mechanism for the temporal regulation of PG cleavage at the cell division site, as FtsA
383 and FtsZ are the key components of the constriction ring at the septum site (15, 18, 27, 32-36).
384 However, the identity of this density and the association of FtsEX with other Fts components for
385 divisome formation warrant further investigation to fully elucidate the role of FtsEX in bacterial cell
386 division.
387
388 In combination with previous studies on the inactivated EnvC (22) and AmiB activation by
389 *Pae*FtsEX (26), we propose a working model that may be conserved across Gram-negative FtsEX
390 systems (**Figure 6**). Firstly, physiological ATP stabilizes the formation of a functional FtsEX
391 regulator with low basal ATP hydrolysis activity. Secondly, the inactivated EnvC approaches the
392 periplasmic space via the relatively flexible PLD domain of FtsEX, which adopts a highly
393 asymmetric conformation, as shown in the inactivated EnvC structure (22). Thirdly, upon full
394 recognition by FtsEX, considering the presence of ATP in cell and a symmetrical conformation
395 defined within the context of a full-length FtsEX complex, recruited EnvC is compelled to adopt a
396 relatively symmetrical conformation, involving squeezing of the coiled-coil domain to facilitate the
397 release of the LytM domain; With EnvC engagement, the ATPase activity of FtsEX is fully activated.
398 Finally, the released LytM recruits amidases through direct interaction, consequently removing the
399 blocking helix from the catalytic site and activating PG cleavage. Remarkably, expansion of the

400 coiled-coil domain in EnvC would place the amidase domain ~300 Å over the inner membrane of
401 the Gram-negative bacteria (as here seen in *E. coli*, and also in *P. aeruginosa* (26)), compatible
402 with the location of the septal PG (26) and avoiding damages into the non-septal cell wall.
403 Throughout this process, ATP binding appears to be sufficient, with ATP hydrolysis potentially
404 serving as a driving force for the release of EnvC and amidases from FtsEX, allowing them to be
405 recycled to a normal ABC transporter. This transporter by itself may play additional roles, such as
406 antibiotic resistance, as suggested by previous studies (22). For the temporal regulation of PG
407 cleavage, the potential interaction between FtsEX and FtsA/FtsZ, as indicated in this study and
408 previous genetic research (17, 27), could bridge the PG-cleaving complex with septum constriction
409 ring, facilitating precise cell division at the septum site. This model provides a potential conserved
410 mechanism for PG cleavage activation by FtsEX and illuminates its temporal regulation. Although
411 further validation is required, our results offer valuable biochemical and structural insights that
412 complement and elucidate decades of genetic research in *E. coli* and other Gram-negative bacteria.
413

414 **Materials and Methods**

415 **Cloning and Mutagenesis**

416 The primers and templates utilized in this study are listed in **Table supplement 1**. To generate the
417 PCR amplicon containing FtsEXs in genomic DNA of *Escherichia coli* Str *K-12 MG1655*,
418 *Streptococcus pneumoniae str. D39*, *Bacillus_subtilis_subsp_subtilis_ATCC_23857*, and
419 *Pseudomonas aeruginosa ATCC 47085D*. ClonExpress II One Step Cloning Kit (Vazyme) was
420 used, followed by purification. After purification through gel electrophoresis, the resulting product
421 was ligated to pTD68 vector (PMID: 20300061) digested with the Nde I and Hind III enzymes to
422 produce pTD68 [PT7::his6-FtsEX]. The construction of pET28-sumo (PT7:his6-sumo-
423 *Eco*EnvC∆34), (PT7:his6-sumo-*Eco*AmiB∆22), involved ligating pET28-sumo digested with BamH
424 I and Xho I to a PCR amplicon synthesized by EnvC-F, EnvC-R, AmiB-F, AmiB-R which were also
425 digested with the same enzymes. The plasmids utilized in this study are listed in **Table supplement**
426 **2.** Mutations to *Eco*FtsE was generated utilizing the QuikChange kit (Agilent Technologies), using
427 pTD68 and pET28-sumo as templates and the primers listed in **Table supplement 1**. The
428 mutations were then verified by DNA sequencing.
429

430 **Protein expression, purification of FtsEX complex and their mutants**

431 FtsEX and its mutants are expressed in *E. coli* strain BL21(DE3) pLysS (Invitrogen) using lysogeny
432 broth (LB) supplemented with 50 µg/ml ampicillin and 10 µg/ml chloramphenicol. This is incubated
433 at 37°C until an optical density at 600 nm (OD_{600}) of 0.8 is achieved. Following this, induction with
434 0.5 mM isopropyl-β-D-thiogalactoside (IPTG) takes place at 20°C for 16 hours. The cells are
435 subsequently harvested through centrifugation using a Beckman JLA9-1000 rotor at 5,180 xg and
436 20°C for 15 minutes. Harvested cells are then stored at -80°C.

437
438 For membrane extraction, the frozen cell pellets undergo thawing at 4°C and are resuspended in
439 buffer A, consisting of 50 mM Tris-HCl pH 8.0, 250 mM NaCl, 10% glycerol, and 2 mM ATP/$MgCl_2$.
440 Lysis of the mixture was achieved with a high-pressure homogenizer (AH-100D, ATS). Subsequent
441 centrifugation was performed at 27,000 xg for an hour at 4°C. Following this, solubilization of the
442 membrane takes place in buffer B, containing 50 mM Tris-HCl, 250 mM NaCl, 1.3% n-dodecyl β-
443 D-maltoside (DDM), pH 8.0, 10% glycerol, and 2 mM ATP/$MgCl_2$, and agitated for 2 hours at 4°C.
444 Post a 30-minute centrifugation at 100,000 xg, the solubilized membrane fraction gets incubated
445 with TALON SuperFlow resin (Takara 635502) for 1 hours at 4°C and was later washed using buffer
446 B supplemented with 20 mM imidazole. The present detergent is substituted by a peptide
447 (GenScript) to form peptidiscs, employing the "on-beads" method (37, 38) with a final peptide
448 concentration of 1mg/ml. The FtsEX complex, reconstituted in the peptidiscs, is washed using
449 buffer B inclusive of 20 mM imidazole and eluted with buffer B rich in 200 mM imidazole. The
450 purified protein is directed through a gel filtration chromatography column (Superose 6 increase
451 10/300) and is eluted with buffer C, which includes 25 mM Tris-HCl, 150 mM NaCl, pH 8.0, and 2
452 mM ATP/$MgCl_2$. The fractions bearing the FtsEX complex are combined together, concentrated to
453 3 mg/ml by concentrator (Amicon® Ulyra-15 100kDa), and preserved at -80°C for further protein
454 interaction, pull-down, and ATP hydrolysis assay.
455
456 **Protein expression, purification of EnvC, AmiB**
457 For the expression of EnvC, AmiB and their respective variants, the *E. coli* strain BL21(DE3) pLysS
458 was employed. These cells were cultured in LB medium with 50 μg/ml kanamycin at 37°C. Once
459 the OD_{600} reached a value of 0.6, induction was facilitated by the addition of IPTG to achieve a final
460 concentration of 0.5 mM, and this was maintained for 16 hours at 20°C. Following the induction,
461 cells were harvested through centrifugation using a JLA9-1000 rotor in a Beckman centrifuge at
462 5,000 rpm and 20°C for a duration of 15 minutes. The resulting pellets were stored at -80°C. For
463 further processing, these frozen pellets were brought to 4°C for thawing, using buffer C (50 mM
464 Tris-HCl pH 8.0, 150 mM NaCl, and 10% glycerol) and then subjected to lysis via a high-pressure
465 homogenizer (AH-100D, ATS). Subsequent centrifugation was performed at 27,000 xg for an hour
466 at 4°C. The resultant supernatant was incubated with TALON resin, followed by a wash using buffer
467 C complemented with 20 mM imidazole. Post-washing, the His-tagged SUMO protease Ulp1 was
468 introduced to the resin-buffer at a ratio of 0.1 mg Ulp1 for every liter of culture, facilitating the
469 cleavage of the SUMO tag over 2 hours at ambient temperature. The processed samples were
470 isolated, concentrated, and then passed through the Superose 6 increase 10/300 column
471 previously balanced in buffer D which includes 25 mM Tris-HCl, 150 mM NaCl, pH 8.0. Target
472 protein was confirmed using SDS-PAGE, further concentrated up to 3 mg/ml, and stored at -80°C.
473

474 **Analyzing the Impact of ATP on the FtsEX Complex**

475 Expression and purification of FtsEXs which from *Escherichia coli (Eco)*, *Streptococcus*
476 *pneumoniae (Sp)*, *Bacillus_subtilis (Bs)*, and *Pseudomonas aeruginosa (Pae)* followed the
477 procedure above. For the ATP-free FstEXs purification, the whole process excludes ATP. For the
478 samples of FtsEXs with ATP or ATP analogs, 2 mM ATP or ATP analogs present in the purification
479 process. The processed samples of *Sp*FtsEX, *Bs*FtsEX, *Pae*FtsEX were concentrated, and then
480 passed through the Superose 6 increase 10/300 column previously balanced in buffer which
481 includes 25 mM Tris-HCl, 150 mM NaCl, pH 8.0 with or without 2 mM ATP. The eluted proteins
482 profiles were confirmed using SDS-PAGE gel. For the *Eco*FtsEX/EnvC samples purification add
483 EnvC with final concentration 1mg/ml after FtsEX reconstituted in the peptidiscs. The eluted ATP-
484 free *Eco*FtsEX sample was performed at 12,000 xg for 15 min at 4°C due to persistent precipitate
485 appearing in the eluted sample. Confirming the supernatant and precipitate using SDS-PAGE gel.
486

487 **Protein interaction assay**

488 To explore the interaction between FtsEX and EnvC, we employed affinity chromatography with
489 TALON resin. Specifically, 15 µg of FtsEX or its ATPase-defective variants were introduced to the
490 resin pre-equilibrated at room temperature, utilizing a Micro Gravity Column, for a 15-minute
491 duration. After washing away unbound FtsEX with 100 µl of buffer E (50 mM Tris-HCl pH 8.0, 150
492 mM NaCl, 10% glycerol, and 2 mM $MgCl_2$) supplemented with 5 mM imidazole (to get rid of the
493 extra ATP present in the protein), we incorporated 5 µg of EnvC diluted in 60 µl of the
494 aforementioned buffer in the presence and absence of ATP or ATP analogs. This mixture was
495 incubated for an additional 10 minutes. Subsequently, the beads were rinsed with buffer E
496 supplemented with 5 mM imidazole in the presence and absence of ATP or ATP analogs. To elute
497 the bound proteins and possible interaction partners, we utilized 20 µl of buffer E with a
498 concentration of 300 mM imidazole, either with or without 2 mM ATP or ATP analogs. Eluted
499 proteins were then analyzed using SDS-PAGE.
500

501 To explore the interactions between FtsEX/EnvC and AmiB, 20 µg of FtsEX/EnvC or its ATPase-
502 deficient variants, $FtsE^{E163Q}X$/EnvC, were added to the TALON resin. This was done either in the
503 presence or absence of 2 mM ATP or ATP analogs and incubated at room temperature for 15
504 minutes. Any free FtsEX/EnvC or $FtsE^{E163Q}X$/EnvC was removed by washing the resin with 100 µl
505 of buffer E containing 5 mM imidazole. Following this, 10 µg of AmiB were introduced to the resin
506 with or without 2 mM ATP or ATP analogs. After a 10-minute incubation, a triple wash was executed
507 using 100 µl of buffer E supplemented with 5 mM imidazole, either with or without 2 mM ATP or
508 ATP analogs . Finally, bound proteins were eluted using 20 µl of buffer E supplemented with 300
509 mM imidazole, either with or without 2 mM ATP or ATP analogs, and the elution profile was
510 assessed via SDS-PAGE.

511

512 **Reconstitution of FtsEX complexes**

513 For the reconstitution of the FtsEX-EnvC complex, an excess of EnvC, three times the amount of
514 FtsEX, was introduced to the resin-bound FtsEX-peptidiscs during the purification process. This
515 mixture was allowed to interact at room temperature for 15 minutes. Subsequent to this incubation,
516 any free EnvC was removed by washing with buffer A containing 20 mM imidazole. The FtsEX-
517 EnvC complex was subsequently eluted from the resin using buffer A supplemented with 200 mM
518 imidazole. This eluted protein was applied to additional purification through gel filtration on a
519 Superose 6 increase 10/300 column, equilibrated in buffer B. Fractions containing the FtsEX-EnvC
520 complex were assessed using SDS-PAGE, combined, concentrated to a concentration of 3 mg/ml,
521 and stored at -80°C.

522

523 For the reconstitution of the AmiB-EnvC-FtsEX supercomplex, AmiB was mixed with the FtsEX-
524 EnvC complex in peptidiscs, at a 3:1 ratio. Following a 15-minute incubation, the supercomplex
525 was further purified via gel filtration. Fractions encompassing the FtsEX-EnvC-AmiB complex were
526 collected, concentrated to 3 mg/ml, and subsequently stored at -80°C.

527

528 **ATP hydrolysis assay**

529 To assess the ATPase activity of FtsEX and its mutants or complxes, we employed the malachite
530 green phosphate assay (39). We introduced 2 µg of FtsEX with or without 0.7 µg of EnvC or 0.7 µg
531 AmiB of following 0.8 µg of EnvC into a 20 µl reaction buffer comprising 25 mM Tris-HCl (pH 8.0),
532 150 mM NaCl, and 2 mM ATP/$MgCl_2$. For the elucidation of the Michaelis-Menten constants,
533 varying concentrations of ATP/$MgCl_2$, ranging from 0.05 to 5 mM, were utilized to initiate the
534 enzymatic reaction. After a 10-minute incubation at 37°C, 80 µl of the Malachite Green-Ammonium
535 Molybdate (MG-AG) solution was added and the resultant mixture was quickly vortexed to
536 deactivate the enzyme. A brief 2-minute incubation was followed by the addition of 10 µl of a 34%
537 (w/v) sodium citrate solution, with a subsequent vortexing step. Absorbance was then recorded at
538 650 nm after a 5-minute interval. Quantification of released inorganic phosphate (Pi) was achieved
539 using a calibration curve derived from known Pi concentrations in a K_2HPO_4 solution. Data
540 processing and curve fitting to the Michaelis-Menten equation were conducted utilizing Microsoft
541 Excel in conjunction with GraphPad Prism 9.

542

543 **Negative staining imaging of FtsE^{E163Q}X-EnvC-AmiB complex**

544 For negative staining of the FtsE^{E163Q}X-EnvC-AmiB sample, it was diluted to a concentration of
545 0.01 mg/ml. A 5 µl aliquot of the sample was deposited onto a 300 mesh copper grid coated with
546 carbon film (EMS). After allowing the sample to interact with the grid for 60 seconds, any surplus
547 was carefully blotted away using filter paper. The grid was then washed with 5 µl of Uranyless EM

548 Stain (EMS). Subsequent to the washing step, the grid was stained by applying another 5 µl of the
549 Uranyless EM Stain for 120 seconds. Excess stain was again removed with filter paper. The
550 prepared grid was left to air-dry under ambient conditions for approximately 15 minutes. Imaging
551 of the sample was executed with a Tecnai 12 microscope (FEI), operating at 120kV with a LaB6
552 source, and magnification set to 52, 000 x.
553
554 **Cryo-Electron microscopy sample preparation and data acquisition**
555 To prepare the sample, 3.5 µl of the protein sample at a concentration of 3 mg/ml was applied to
556 Quantifoil holey carbon grids (R1.2/1.3, 400 mesh) that were glow-discharged. To obtain the ATPγS
557 -bound complex, the sample was incubated at 37°C for 8 minutes with 3mM ATPγS-2mM Mg^{2+}
558 (FtsEX) or 2 mM ATP-Mg^{2+} ($FtsE^{E163Q}X$/EnvC) before freezing. The grids were blotted for 3.5-4
559 seconds with 100% relative humidity and then plunge-frozen in liquid ethane that was cooled by
560 liquid nitrogen using a Vitrobot System (Gatan).
561
562 Cryo-electron microscopy data was collected at liquid nitrogen temperature using a Titan Krios
563 electron microscope (Thermo Fisher Scientific), equipped with a K3 Summit direct electron detector
564 (Gatan) and GIF Quantum energy filter. All cryo-EM movies were recorded in counting mode with
565 SerialEM4 (40) with a slit width of 20 eV from the energy filter. Movies were acquired at nominal
566 magnifications of 81k x, which corresponded to a calibrated pixel size of 1.06 Å on the specimen
567 level. The total exposure time for each movie was 5 seconds, resulting in a total dose range of 35-
568 39 electrons per $Å^2$, fractionated into 34 frames. Additional electron microscopy data collection
569 parameters can be found in **Table supplement 3**.
570
571 **Cryo-Electron microscope image processing.**
572 For electron microscopy (EM) data processing, CryoSPARC (41) was utilized. Dose-fractionated
573 movies, captured with a K3 Summit direct electron detector, was first applied to motion correction
574 using MotionCor2 (42). A sum of all frames from each movie was generated applying a dose-
575 weighting scheme. This sum was utilized for all subsequent image-processing steps, except for
576 defocus determination. For that, CTFFIND4 (43) was used on the non-dose-weighted summed
577 images from all movie frames. The initial particle selection was achieved using the blob picker,
578 which was subsequently refined by the template picker. The steps of 2D and 3D classification, as
579 well as 3D refinement, were carried out using the "2D Classification", "Ab-initial Reconstruction",
580 and "Heterogeneous Refinement" functions. For further refinement, both the "Homogeneous
581 Refinement" and "Non-Uniform Refinement" functions were employed. The overall resolutions was
582 determined using the gold-standard Fourier shell correlation (FSC) threshold of 0.143. Lastly, the
583 local resolution was assessed via the "Local Resolution Estimation" tool.
584

585 **Model building and refinement for FtsEX and its complex with EnvC**
586 The cryo-EM maps of the ATPγS-bound FtsEX and ATP-bound FtsE^{E163Q}X/EnvC complexes were
587 resolved at resolutions of 3.7 Å and 3.4 Å, respectively, with sufficient quality to enable accurate
588 model building for the TMD domain, FtsE, and a portion of the PLD region (see **Figure supplement**
589 **3** and **Figure supplement 6** for details), leaving only the N-terminal region of FtsX, including
590 residues 1-52, not modeled.
591
592 Initial models for FtsE and FtsX were generated using the AlphaFold program (41). Subsequently,
593 the FtsEX models were rigid-body fitted into the cryo-EM map density using UCSF Chimera
594 software (44). These initial models were then refined manually within Coot (45). Restraints for
595 ATPγS were generated using the phenix_elbow program, employing its isomeric SMILES string
596 files obtained from the PDB Chemical Component Dictionary via Ligand Expo. Further refinement
597 was performed using Phenix (46), including 'minimization_global' and 'Real-space refinement'
598 protocols. Multiple rounds of manual adjustments in Coot, in conjunction with real-space refinement
599 in Phenix, were carried out to obtain the final model. Model validation was performed using
600 Ramachandran plots, MolProbity scores, and Clash scores in Phenix (46) (details provided in **Table**
601 **supplement 3**).
602
603 In the case of the FtsE^{E163Q}X/EnvC/ATP complex structure, the initial models for EnvC was derived
604 from AlphaFold (47) and our resolved FtsEX structure was used as initial model for FtsEX part.
605 These initial models were fitted into the cryo-EM map of the FtsE^{E163Q}X/EnvC/ATP complex using
606 UCSF Chimera (44). Subsequent manual adjustments were performed within Coot (45), and the
607 Glu163 was replaced with Gln. Similar to the ATPγS-containing complex, restraints for ATP were
608 generated using the phenix_elbow program. The model was refined using phenix software (46),
609 incorporating 'minimization_global' and 'Real-space refinement' procedures. The final model was
610 refined through multiple iterations of manual adjustments in Coot (45), alongside real-space
611 refinement in Phenix. Model quality assessment included Ramachandran plots, MolProbity scores,
612 and Clash scores, with detailed results provided in **Table supplement 3 (46)**.
613

614 **Acknowledgments**
615 We appreciate the contributions of Yibei Xiao and Zhaoxing Li from China Pharmaceutical
616 University, whose expertise in Mass Spectrometry greatly enhanced our research. Furthermore,
617 we thank all Luo lab members for their constructive comments throughout the course of this study.
618
619 **Funding:** This work was supported by the National University of Singapore Start-up grant to M. L.,
620 the Ministry of Education Tier 2 Grant to M.L. and L.-T. S. (MOE-T2EP30222-0015, MOE-
621 T2EP30220-0012, and T2EP30123-0017), the National Medical Research Council grant to L.-T. S.

(A-8001581-00-00), and the National Research Foundation grant to M.L. and L.-T. S. (NRF-CRP22-2019-0001 and NRFF11-2019-0005). The work in Spain is supported by grants PID2020-115331GB-100 funded by MCIN/AEI/10.13039/501100011033 and CRSII5_198737/1 by the Swiss National Science Foundation to J.A.H.

Data and materials availability: Two three-dimensional cryo-EM density maps of FtsEX and its complexes with EnvC have been deposited in the Electron Microscopy Data Bank under accession codes: EMD-37324 (ATPγS-bound FtsEX); EMD-37325(ATP-bound FtsE^{E163Q}X with EnvC). Two atomic models have been deposited in the Protein Data Bank under accession codes 8W6I (ATPγS bound FtsEX), and 8W6J (ATP-bound FtsE^{E163Q}X/EnvC). All data presented in this study are provided within the main text and supplementary materials, or readily accessible upon request.

References

1. T. Do, J. E. Page, S. Walker, Uncovering the activities, biological roles, and regulation of bacterial cell wall hydrolases and tailoring enzymes. *J Biol Chem* **295**, 3347-3361 (2020).
2. A. Typas, M. Banzhaf, C. A. Gross, W. Vollmer, From the regulation of peptidoglycan synthesis to bacterial growth and morphology. *Nat Rev Microbiol* **10**, 123-136 (2011).
3. P. D. A. Rohs, T. G. Bernhardt, Growth and Division of the Peptidoglycan Matrix. *Annu Rev Microbiol* **75**, 315-336 (2021).
4. S. Du, J. Lutkenhaus, Assembly and activation of the Escherichia coli divisome. *Mol Microbiol* **105**, 177-187 (2017).
5. S. Du, J. Lutkenhaus, At the Heart of Bacterial Cytokinesis: The Z Ring. *Trends Microbiol* **27**, 781-791 (2019).
6. J. Lutkenhaus, S. Du, E. coli Cell Cycle Machinery. *Subcell Biochem* **84**, 27-65 (2017).
7. Z. Lyu *et al.*, FtsN maintains active septal cell wall synthesis by forming a processive complex with the septum-specific peptidoglycan synthases in E. coli. *Nat Commun* **13**, 5751 (2022).
8. T. A. Cameron, W. Margolin, Insights into the assembly and regulation of the bacterial divisome. *Nat Rev Microbiol* 10.1038/s41579-023-00942-x (2023).
9. M. J. Tsang, T. G. Bernhardt, Guiding divisome assembly and controlling its activity. *Curr Opin Microbiol* **24**, 60-65 (2015).
10. M. J. Tsang, A. A. Yakhnina, T. G. Bernhardt, NlpD links cell wall remodeling and outer membrane invagination during cytokinesis in Escherichia coli. *PLoS Genet* **13**, e1006888 (2017).
11. T. Uehara, T. G. Bernhardt, More than just lysins: peptidoglycan hydrolases tailor the cell wall. *Curr Opin Microbiol* **14**, 698-703 (2011).
12. T. Uehara, K. R. Parzych, T. Dinh, T. G. Bernhardt, Daughter cell separation is controlled by cytokinetic ring-activated cell wall hydrolysis. *EMBO J* **29**, 1412-1422 (2010).
13. M. Alcorlo, S. Martinez-Caballero, R. Molina, J. A. Hermoso, Regulation of Lytic Machineries by the FtsEX Complex in the Bacterial Divisome. *Subcell Biochem* **99**, 285-315 (2022).
14. S. Pichoff, S. Du, J. Lutkenhaus, Roles of FtsEX in cell division. *Res Microbiol* **170**, 374-380 (2019).

664 15. S. Du, S. Pichoff, J. Lutkenhaus, Roles of ATP Hydrolysis by FtsEX and Interaction with FtsA
665 in Regulation of Septal Peptidoglycan Synthesis and Hydrolysis. *mBio* **11** (2020).
666 16. D. C. Yang *et al.*, An ATP-binding cassette transporter-like complex governs cell-wall
667 hydrolysis at the bacterial cytokinetic ring. *Proc Natl Acad Sci U S A* **108**, E1052-1060
668 (2011).
669 17. S. Du, S. Pichoff, J. Lutkenhaus, FtsEX acts on FtsA to regulate divisome assembly and
670 activity. *Proc Natl Acad Sci U S A* **113**, E5052-5061 (2016).
671 18. S. Du, W. Henke, S. Pichoff, J. Lutkenhaus, How FtsEX localizes to the Z ring and interacts
672 with FtsA to regulate cell division. *Mol Microbiol* **112**, 881-895 (2019).
673 19. S. J. Arends, R. J. Kustusch, D. S. Weiss, ATP-binding site lesions in FtsE impair cell division.
674 *J Bacteriol* **191**, 3772-3784 (2009).
675 20. M. Reddy, Role of FtsEX in cell division of Escherichia coli: viability of ftsEX mutants is
676 dependent on functional SufI or high osmotic strength. *J Bacteriol* **189**, 98-108 (2007).
677 21. K. L. Schmidt *et al.*, A predicted ABC transporter, FtsEX, is needed for cell division in
678 Escherichia coli. *J Bacteriol* **186**, 785-793 (2004).
679 22. J. Cook *et al.*, Insights into bacterial cell division from a structure of EnvC bound to the
680 FtsX periplasmic domain. *Proc Natl Acad Sci U S A* **117**, 28355-28365 (2020).
681 23. D. Mavrici *et al.*, Mycobacterium tuberculosis FtsX extracellular domain activates the
682 peptidoglycan hydrolase, RipC. *Proc Natl Acad Sci U S A* **111**, 8037-8042 (2014).
683 24. B. E. Rued *et al.*, Structure of the Large Extracellular Loop of FtsX and Its Interaction with
684 the Essential Peptidoglycan Hydrolase PcsB in Streptococcus pneumoniae. *mBio* **10**
685 (2019).
686 25. Y. Fu, K. E. Bruce, B. Rued, M. E. Winkler, D. P. Giedroc, 1H, 13C, 15N resonance
687 assignments of the extracellular loop 1 domain (ECL1) of Streptococcus pneumoniae D39
688 FtsX, an essential cell division protein. *Biomol NMR Assign* **10**, 89-92 (2016).
689 26. X. Xu *et al.*, Mechanistic insights into the regulation of cell wall hydrolysis by FtsEX and
690 EnvC at the bacterial division site. *Proc Natl Acad Sci U S A* **120**, e2301897120 (2023).
691 27. B. D. Corbin, Y. Wang, T. K. Beuria, W. Margolin, Interaction between cell division proteins
692 FtsE and FtsZ. *J Bacteriol* **189**, 3026-3035 (2007).
693 28. X. Ou *et al.*, ATP Can Efficiently Stabilize Protein through a Unique Mechanism. *JACS Au* **1**,
694 1766-1777 (2021).
695 29. S. Sridharan *et al.*, Proteome-wide solubility and thermal stability profiling reveals distinct
696 regulatory roles for ATP. *Nat Commun* **10**, 1155 (2019).
697 30. S. C. Lee *et al.*, Nano-encapsulated Escherichia coli Divisome Anchor ZipA, and in Complex
698 with FtsZ. *Sci Rep* **9**, 18712 (2019).
699 31. S. C. Lee *et al.*, A method for detergent-free isolation of membrane proteins in their local
700 lipid environment. *Nat Protoc* **11**, 1149-1162 (2016).
701 32. E. Godino, C. Danelon, Gene-Directed FtsZ Ring Assembly Generates Constricted
702 Liposomes with Stable Membrane Necks. *Adv Biol (Weinh)* **7**, e2200172 (2023).
703 33. C. Ortiz, P. Natale, L. Cueto, M. Vicente, The keepers of the ring: regulators of FtsZ
704 assembly. *FEMS Microbiol Rev* **40**, 57-67 (2016).
705 34. P. Szwedziak, Q. Wang, T. A. Bharat, M. Tsim, J. Lowe, Architecture of the ring formed by
706 the tubulin homologue FtsZ in bacterial cell division. *Elife* **3**, e04601 (2014).
707 35. S. Rueda, M. Vicente, J. Mingorance, Concentration and assembly of the division ring
708 proteins FtsZ, FtsA, and ZipA during the Escherichia coli cell cycle. *J Bacteriol* **185**, 3344-
709 3351 (2003).
710 36. H. P. Erickson, M. Osawa, FtsZ Constriction Force - Curved Protofilaments Bending
711 Membranes. *Subcell Biochem* **84**, 139-160 (2017).

37. M. L. Carlson *et al.*, The Peptidisc, a simple method for stabilizing membrane proteins in detergent-free solution. *Elife* **7** (2018).
38. G. Angiulli *et al.*, New approach for membrane protein reconstitution into peptidiscs and basis for their adaptability to different proteins. *Elife* **9** (2020).
39. P. A. Lanzetta, L. J. Alvarez, P. S. Reinach, O. A. Candia, An improved assay for nanomole amounts of inorganic phosphate. *Anal Biochem* **100**, 95-97 (1979).
40. D. N. Mastronarde, Automated electron microscope tomography using robust prediction of specimen movements. *J Struct Biol* **152**, 36-51 (2005).
41. A. Punjani, J. L. Rubinstein, D. J. Fleet, M. A. Brubaker, cryoSPARC: algorithms for rapid unsupervised cryo-EM structure determination. *Nat Methods* **14**, 290-296 (2017).
42. S. Q. Zheng *et al.*, MotionCor2: anisotropic correction of beam-induced motion for improved cryo-electron microscopy. *Nat Methods* **14**, 331-332 (2017).
43. A. Rohou, N. Grigorieff, CTFFIND4: Fast and accurate defocus estimation from electron micrographs. *J Struct Biol* **192**, 216-221 (2015).
44. E. F. Pettersen *et al.*, UCSF Chimera--a visualization system for exploratory research and analysis. *J Comput Chem* **25**, 1605-1612 (2004).
45. P. Emsley, K. Cowtan, Coot: model-building tools for molecular graphics. *Acta Crystallogr D Biol Crystallogr* **60**, 2126-2132 (2004).
46. P. D. Adams *et al.*, PHENIX: a comprehensive Python-based system for macromolecular structure solution. *Acta Crystallogr D Biol Crystallogr* **66**, 213-221 (2010).
47. J. Jumper *et al.*, Highly accurate protein structure prediction with AlphaFold. *Nature* **596**, 583-589 (2021).

Figures

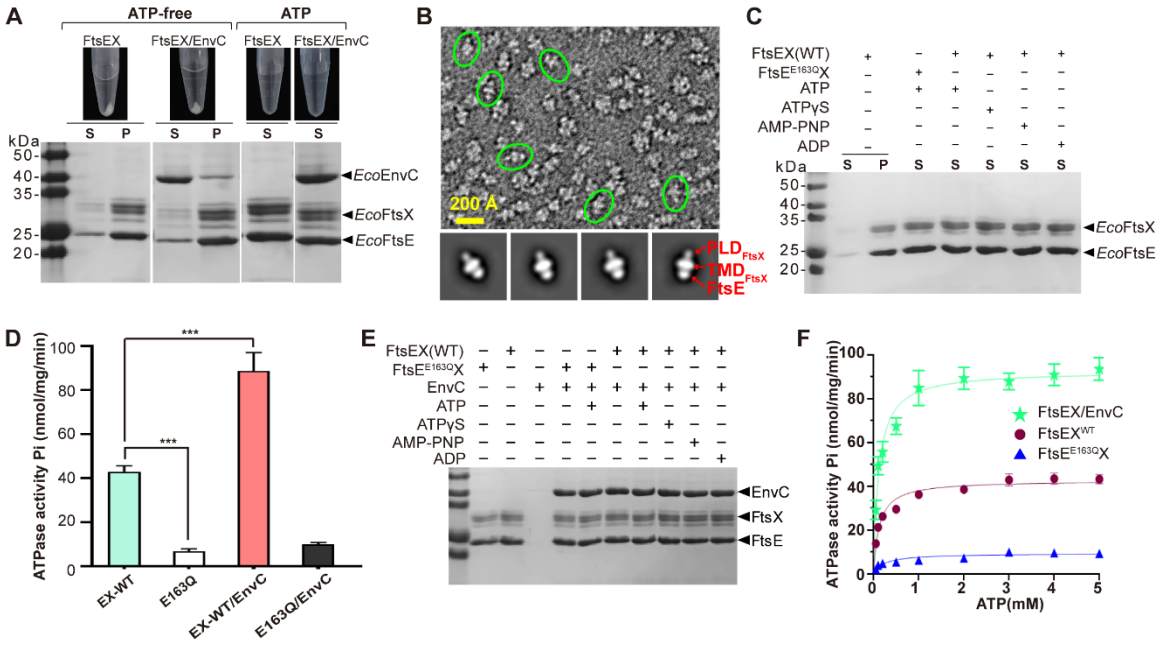

Figure 1. Biochemical reconstitution of *Eco*FtsEX and *Eco*FtsEX/EnvC complexes. (A) Evaluation of ATP's impact on FtsEX and FtsEX/EnvC complexes. Purified FtsEX and FtsEX/EnvC complexes undergo precipitation in the absence of ATP but form stable complexes when ATP is present during purification. S: Supernatant, P: Precipitate. **(B)** Representative negative staining

image and 2D average of FtsEX samples purified in the presence of ATP, with FtsEX highlighted in green. The FtsE subunit, Transmembrane Domain (TMD), and Periplasmic Domain (PLD) of FtsX are clearly visible. **(C)** Assessment of ATP and ATP analogs' influence on the stability of FtsEX complex formation. ATP and ATP analogs contribute to the stabilization of the FtsEX complex. S: Supernatant, P: Precipitate. (**D**) Assessment of ATPase activity in FtsEX and FtsEX mutants, with and without EnvC. Notably, the FtsE^{E163Q}X mutants exhibit significantly reduced ATPase activity. Data represent an average of three replicates, with error bars indicating mean ± SD. Statistical analysis performed using a two-tailed unpaired t-test; ***P < 0.0005. (**E**)**.** Pull-down study illustrating EnvC binding to FtsEX or its ATPase mutant in the presence or absence of ATP or ATP analogs. The initial FtsEX or FtsE^{E163Q}X added to the resin contains 2 mM ATP, the ATP was subsequently removed by the wash buffer. (**F**) ATPase activity comparison between FtsEX and the FtsEX/EnvC complex in peptidiscs. Data represent an average of three replicates, with error bars indicating mean ± SD.

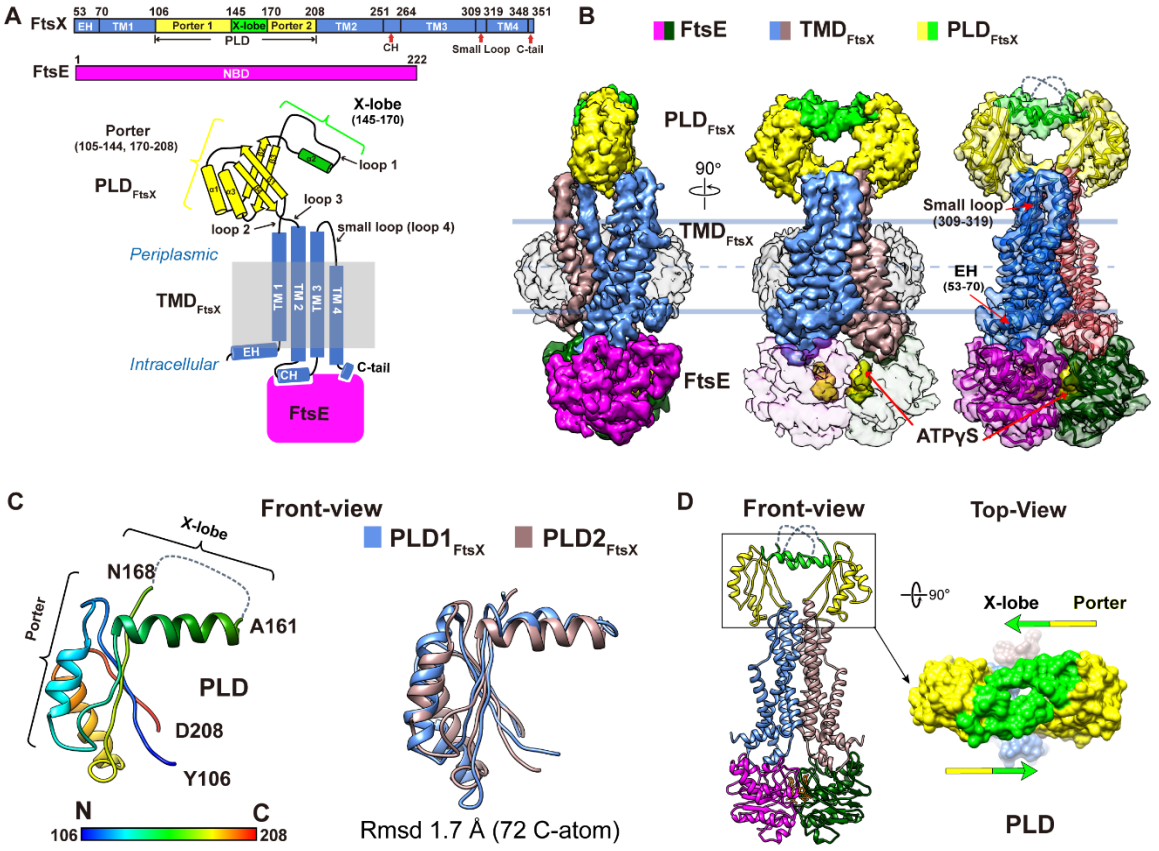

Figure 2. Cryo-EM study of *Eco*FtsEX complex in peptidiscs. (**A**) Topological diagram of FtsEX, highlighting the α helices represented as cylinders and β sheets depicted as arrows. Color scheme: FtsE (magenta and dark green), FtsX (cornflower blue), Porter of PLD_{FtsX} (yellow), and X-lobe of PLD_{FtsX} (green). CH: coupling helix, EH: elbow helix. (**B**) Left and middle panels depict the side and front views of the density map of FtsEX, with ATPγS displayed in the front view at 90%

transparency. Ribbon representation of WT FtsEX in the presence of ATPγS with EM density. Color scheme: FtsE (magenta and dark green), FtsX (cornflower blue and rosy brown), Porter of PCD_{FtsX} (yellow), and X-lobe of PLD_{FtsX} (green). EH: elbow helix. (**C**) Left panel presents a rainbow representation of the PLD domain of FtsX, transitioning from blue (N-terminal) to red (C-terminal). Right panel shows a front view overlay of two PLD domains. (**D**) Surface representations of the PLD domains in a top-view configuration, with the Porter of the PLD colored in yellow and the X-lobe in green. In *Eco*FtsEX, the Porter and X-lobe are positioned facing each other.

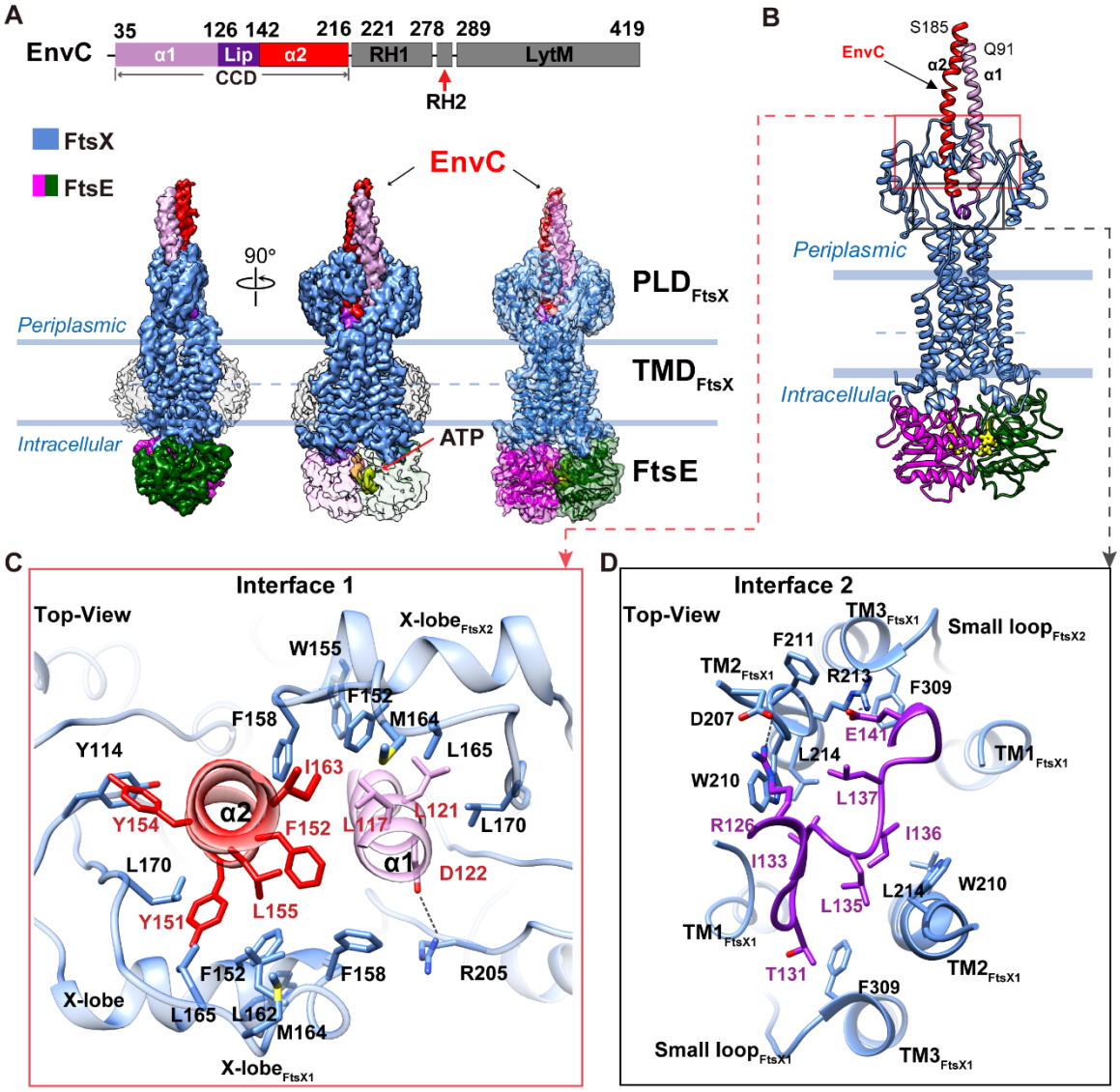

768

769 **Figure 3. Cryo-EM structure of the EnvC-bound *Eco*FtsEX complex.** (**A**) Domain arrangements
770 and the overall structure of FtsEX/EnvC. Left and middle panels display side and front views of the
771 cryo-EM density maps for FtsEX-EnvC complex in the presence of ATP. The right panel presents
772 a ribbon representation of the structural model overlaid with the EM density. In the front-view, FtsE
773 is depicted at 90% transparency to reveal the ATP-binding site. Color scheme of EnvC: α1 (plum),
774 lip (purple), α2 (red), RH1, RH2, and LytM domains (grey). (**B**) EnvC binding to the PLD domain of
775 FtsEX is depicted with ribbon representations. Color scheme: FtsX (cornflower blue), FtsE
776 (magenta/dark green), and EnvC (red). (**C**) **&** (**D**). Top-down views provide a detailed depiction of
777 the interaction between EnvC and FtsEX.

778

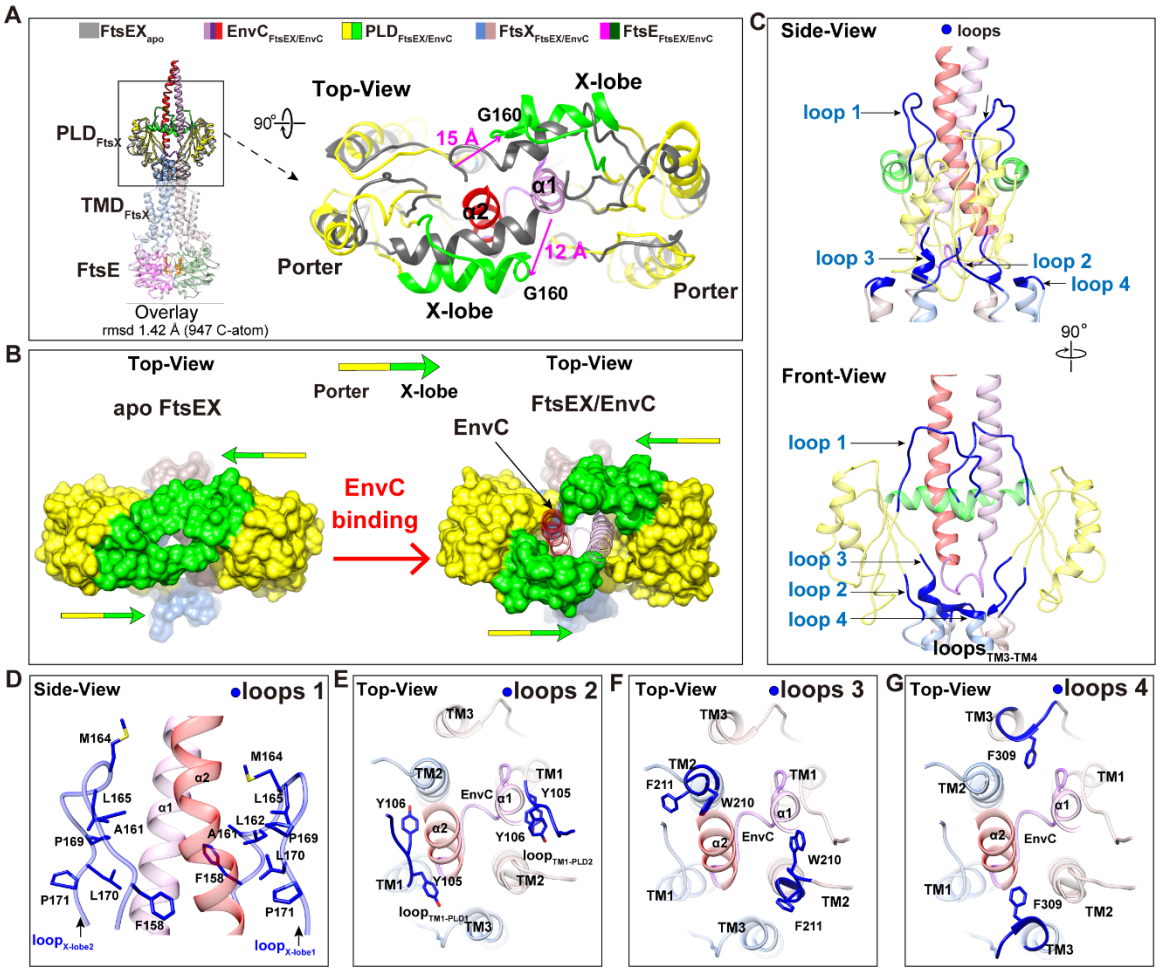

Figure 4. Identification of key loops for EnvC binding in the *Eco*FtsEX/EnvC Complex. (**A**) Overlay of *Eco*FtsEX and *Eco*FtsEX/EnvC complexes, with a focus on the conformational changes in the PLD domain induced by EnvC binding. The overall overlay of *Eco*FtsEX and *Eco*FtsEX/EnvC is depicted in ribbon form. Color scheme: FtsE (magenta and dark green), FtsX (cornflower blue and rosy brown), Porter of PLD$_{FtsX}$ (yellow), and X-lobe of PLD$_{FtsX}$ (green). The TMD and FtsE regions are set at 60% transparency. (**B**) Depiction of the conformational changes in the PLD domains upon EnvC binding. (**C**) Side and front views illustrating the key loops involved in EnvC binding within the *Eco*FtsEX/EnvC complex. Key loops of FtsX, highlighted in blue, are indicated by arrows and labeled. (**D**) Side-view displaying the binding details between EnvC and flexible loops located in the X-lobe (G157-L171). (**E**)**,** (**F**)**, and** (**G**) Top-down views demonstrating the binding details of EnvC and flexible loops positioned between TM1 and PLD (Y105-Q109) (**E**), PLD and TM2 (D208-L214) (**F**), and TM3 and TM4 (Q307-T311) (**G**).

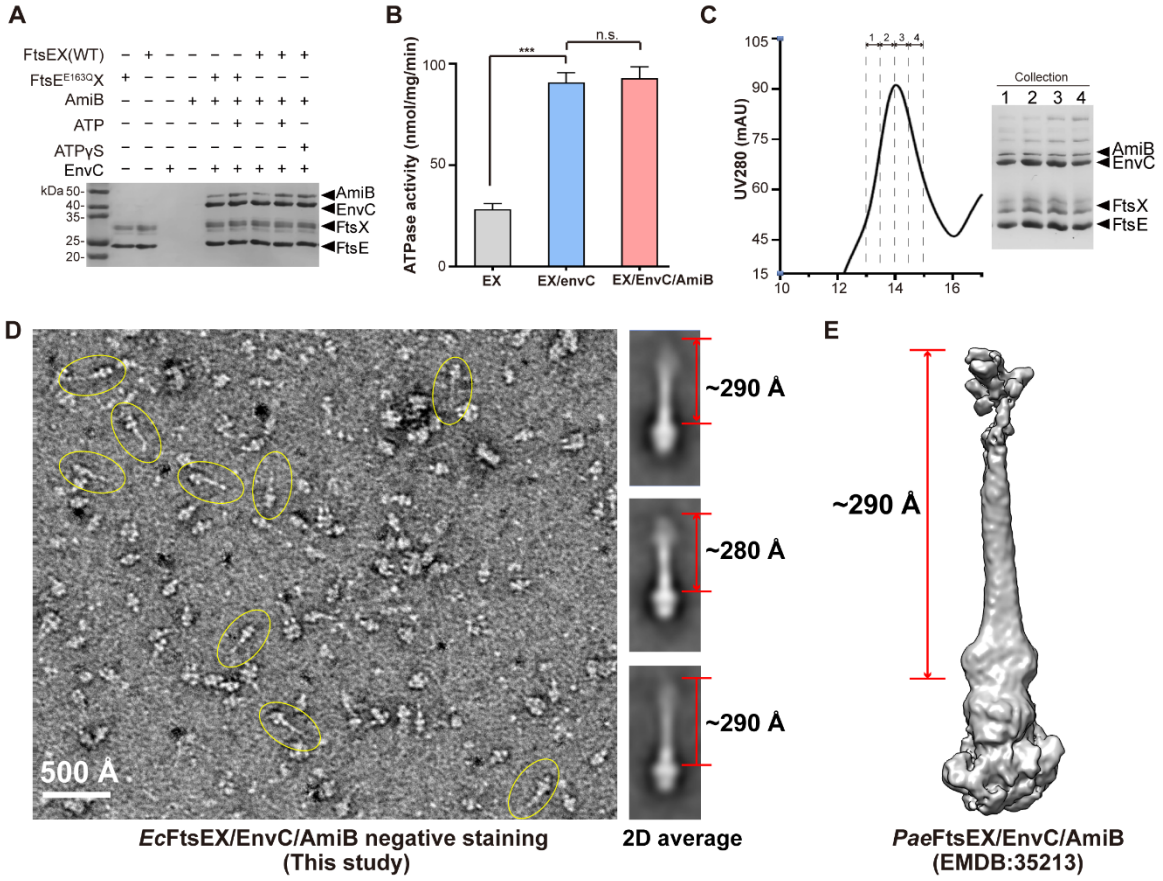

Figure 5. Biochemical reconstitution and negative-staining EM study of the AmiB-Bound *Eco*FtsEX/EnvC Complex. (**A**) Pull-down study illustrating the interaction between AmiB and FtsEX-EnvC or its ATPase mutant, in the presence or absence of ATP or its analogs. The initial FtsEX or FtsE^{E163Q}X added to the resin contains 2 mM ATP, the ATP was subsequently removed by the wash buffer. (**B**) Evaluation of ATPase activity in FtsEX, FtsEX/EnvC, and FtsEX/EnvC/AmiB complexes. Notably, the binding of AmiB does not significantly impact the ATPase activity of FtsEX/EnvC. Data represent an average of three replicates, with error bars indicating mean ± SD. Statistical analysis performed using a two-tailed unpaired t-test; ***P < 0.0005. (**C**) SEC profile and SDS-PAGE gel of purified FtsEX/EnvC/AmiB complex reconstituted in peptidiscs. (**D**) Negative-staining micrograph and 2D average image of *Eco*FtsEX/EnvC/AmiB. (**E**) Cryo-EM density map of *Pae*FtsEX/EnvC/AmiB.

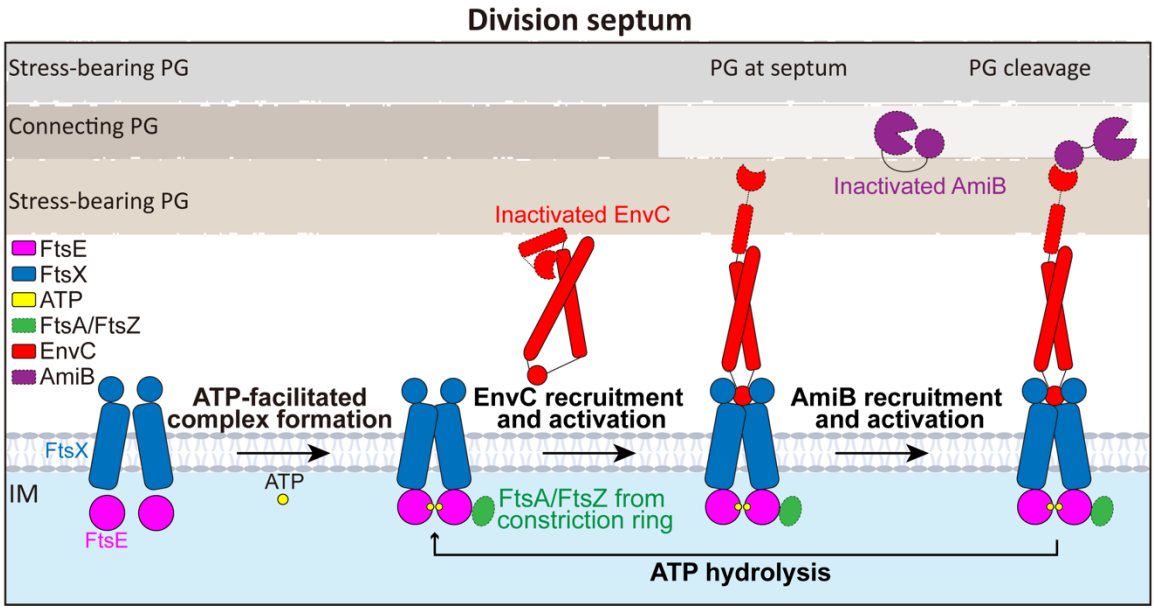

Figure 6. A working model illustrating FtsEX complex formation, recruitment of EnvC and AmiB, and the temporal regulation of PG cleavage activation in Gram-negative bacterial systems. Initially, the presence of physiological ATP stabilizes a fully functional FtsEX complex. Subsequently, the asymmetrical and inactive EnvC approaches the relatively flexible PLD domain of FtsEX. Upon complete recognition by FtsEX, the CCD domain of recruited EnvC undergoes a conformational change to a symmetrical state, involving compression of the coiled-coil domain, facilitating the release of the LytM domain. Interaction with EnvC activates FtsEX's ATPase activity. The liberated LytM recruits amidases through direct interaction with the catalytic domain's blocking helices, leading to the removal of the obstructing helix from the catalytic site and activation of PG cleavage. ATP hydrolysis likely triggers the release of EnvC and AmiB, allowing FtsEX to return to its normal ABC transporter state with a low basal ATPase activity. The potential interaction between FtsEX and the constriction ring component FtsA/FtsZ precisely locates the PG-cleaving complex at the septum for temporal regulation of PG cleavage.